Heliyon

Received:
19 June 2018
Revised:
15 January 2019
Accepted:
26 February 2019

Cite as:
Estibaliz Santiago-Mujica, Stefanie Flunkert, Roland Rabl, Joerg Neddens, Tina Loeffler, Birgit Hutter-Paier. Hepatic and neuronal phenotype of NPC1$^{-/-}$ mice. Heliyon 5 (2019) e01293. doi: 10.1016/j.heliyon.2019.e01293

Hepatic and neuronal phenotype of NPC1$^{-/-}$ mice

Estibaliz Santiago-Mujica [1], Stefanie Flunkert [1], Roland Rabl, Joerg Neddens, Tina Loeffler, Birgit Hutter-Paier*

QPS Austria GmbH, Parkring 12, 8074, Grambach, Austria

* Corresponding author.

E-mail address: Birgit.Hutter-Paier@qps.com (B. Hutter-Paier).

[1] Contributed equally.

Abstract

Niemann-Pick type C disease (NPC) is a fatal autosomal recessive disorder characterized by a defect in the intracellular transport of lipoproteins leading to the accumulation of lipids in diverse tissues. A visceral and neuronal phenotype mimicking human NPC1 disease has been described in NPC1 mutant mice. These mice are by now the most widely used NPC1 rodent model to study NPC and developmental compounds against this devastating disease. Here we characterized NPC1$^{-/-}$ mice for their hepatic and neuronal phenotype to confirm the stability of the phenotype, provide a characterization of disease progression and pinpoint the age of robust phenotype onset. Animals of 4–10 weeks of age were analyzed for general health, motor deficits as well as hepatic and neuronal alterations with a special focus on cerebellar pathology.

Our results show that NPC1$^{-/-}$ mice have a reduced general health at the age of 9–10 weeks. Robust motor deficits can be observed even earlier at 8 weeks of age. Hepatic changes included increased organ weight and cholesterol levels at 6 weeks of age accompanied by severely increased liver enzyme levels. Analysis of NPC1$^{-/-}$ brain pathology showed decreased cholesterol and increased Aβ levels in the hippocampus at the age of 6 weeks. Further analysis revealed a decrease of the cytokine IL-12p70 in the cerebellum along with a very early increase of astrocytosis. Hippocampal IL-12p70 levels were increased at the age of 6 weeks followed by increased activated microglia levels. By the age of 10 weeks, also cerebellar Aβ levels were increased along with strongly reduced Calbindin D-28k levels.

https://doi.org/10.1016/j.heliyon.2019.e01293

Our results validate and summarize the progressive development of the hepatic and neuronal phenotype of NPC1$^{-/-}$ mice that starts with cerebellar astrocytosis, making this mouse model a valuable tool for the development of new compounds against NPC.

List of abbreviations: AAALAC: Association for Assessment and Accreditation of Laboratory Animal Care; ALT: alanine aminotransferase; ANOVA: Analysis of variance; AOI: Area of interest; AP: alkaline phosphatase; APP: Amyloid Precursor Protein; AST: aspartate aminotransferase; CD45: cluster of differentiation 45; CNS: central nervous system; DAPI: 4′,6-Diamidin-2-phenylindol; GFAP: Glial fibrillary acidic protein; IFN-γ: Interferon-gamma; IL-10/12: Interleukin-10/12; KC: keratinocyte chemoattractant; MAP2: microtubuli-associated protein 2; NPC: Niemann-Pick type C; TNF-α: tumor necrosis factor-alpha; WT: wildtype

Keywords: Cell biology, Molecular biology, Neuroscience, Physiology

1. Background

The classical Niemann-Pick type C disease (NPC) is a fatal autosomal recessive disorder that affects approximately 1 in 90,000 live births in western countries while the late-onset form of the disease has an incidence rate of up to 1 in 20,000 (Wassif et al., 2016). Mutations in the NPC1 gene account for approximately 95% while mutations in the NPC2 gene are responsible for the remaining 5% of NPC cases (for review see (Wraith et al., 2009)). NPC1 mutations cause a loss of protein function (Carstea et al., 1997) resulting in a disturbed transport of several lipids like cholesterol, sphingomyelin, glucosylceramide and sphingosine making the NPC1 protein a multi-substrate transporter (Lloyd-Evans and Platt, 2010). NPC1 localizes to the late endosome and the periphery of lysosomes (Zhang et al., 2003) causing increased cholesterol levels in visceral organs but decreased levels in the brains white matter (Vanier, 1983, 1999). Thus, spleen and liver, as well as the brain are almost universally affected, leading to a variable heterogeneous symptomatology and progression (Mengel et al., 2013). The clinical presentation is extremely heterogeneous, with an age of onset ranging from the perinatal period until adult age (Vanier, 2010). Similarly, the lifespan of patients varies between a few days to over 60 years, although a majority of cases die between 10 and 25 years of age (Group et al., 2009).

A visceral and neuronal phenotype mimicking human NPC1 disease has been described in NPC1 mutant mice on a Balb/C background (BALB/cNctr-Npc1<m1N>/J), presenting the first mouse model of NPC1 that has been used for most NPC1 studies since then (Loftus et al., 1997; Zervas et al., 2001). Animals have an almost total absence of the NPC1 protein and display pathological hallmarks

https://doi.org/10.1016/j.heliyon.2019.e01293

of the disease (Loftus et al., 1997). Due to the shortened lifespan of only 10–14 weeks, NPC1$^{-/-}$ mice have a more severe disease progression than the vast majority of patients (Smith et al., 2009).

During the first month of life NPC1$^{-/-}$ mice present only minor phenotypical differences compared to wildtype animals (WTs) like reduced body weight and first signs of neuronal loss (Ong et al., 2001; Nicoli et al., 2016). At 5–6 weeks of age tremor, ataxic gait and motor deficits start. By 7–8 weeks, NPC1$^{-/-}$ mice start losing weight and motor control problems become obvious (Loftus et al., 1997; Voikar et al., 2002; Paul et al., 2004; Li et al., 2005; Smith et al., 2009). NPC1$^{-/-}$ mice present accumulation of unesterified cholesterol in different tissues, abnormalities in lysosomal enzyme levels, increased activity of hepatic enzymes and decreased levels of triacylglycerides (Pentchev et al., 1980; Amigo et al., 2002; Beltroy et al., 2005, 2007; Kulinski and Vance, 2007). At present there is no cure for Niemann-Pick disease, and the only available treatment, Miglustat, can alleviate symptoms but does not cure the disease ((Wraith et al., 2010; Bowman et al., 2015; Sedel et al., 2016; Bowman et al., 2018), for review see (Lyseng-Williamson, 2014)).

In this study, we performed an in-depth biochemical and behavioral characterization over age of NPC1$^{-/-}$ mice to confirm the stability of the phenotype, provide a characterization of disease progression and pinpoint the age of robust phenotype presence in this mouse model which will support future therapeutic strategies.

2. Results

2.1. General health and motor deficits of NPC1$^{-/-}$ mice over age

To evaluate the health status of NPC1$^{-/-}$ mice and wildtype (WT) littermates, animals' body weight and body temperature were measured weekly for 6 weeks. Both NPC1$^{-/-}$ and WT mice showed a similar body weight gain during the first 4 weeks of measurement: the weight gain at 6 weeks of age was maintained more or less constant until mice were 8 weeks old. From 8 weeks onwards, NPC1$^{-/-}$ mice were significantly lighter compared to WT littermates (Fig. 1A). The body temperature stayed constant in both groups until the animals were 9 weeks old. From that time onwards, NPC1$^{-/-}$ mice showed a significantly lower body temperature compared to WT littermates (Fig. 1B).

To evaluate the general activity of NPC1$^{-/-}$ mice, the nesting behavior was measured over age. In WT littermates, an increase in the nesting score during the first two weeks could be observed. Afterwards, the score stayed constant until the age of 10 weeks. On the other hand, NPC1$^{-/-}$ mice showed a similar nesting score at 5 and 6 weeks of age compared to WT littermates. Nonetheless, a significantly disturbed

https://doi.org/10.1016/j.heliyon.2019.e01293

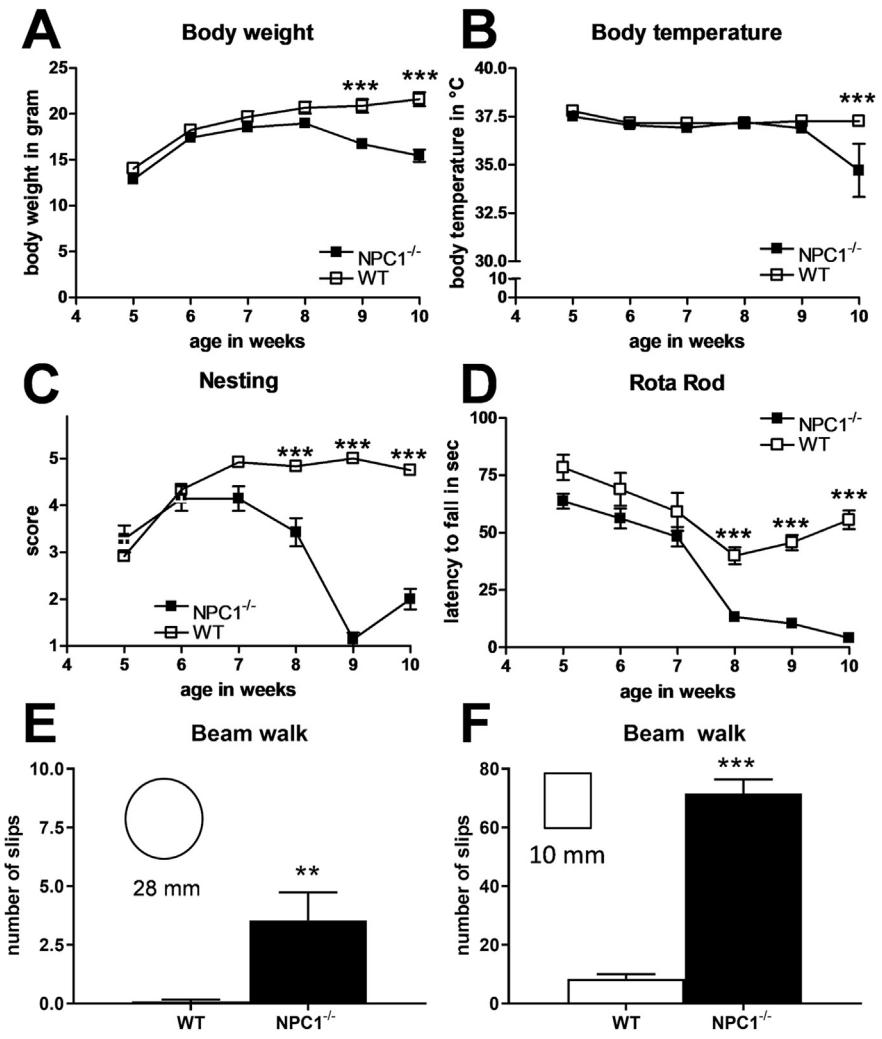

Fig. 1. General health and motor deficits in NPC1$^{-/-}$ mice over age. Body weight in gram (A), body temperature in degree celsius (B), nest building score (C; 5 = perfect nest) and latency to fall off the rotating Rota Rod in seconds (D) of 4−10 week old NPC1$^{-/-}$ mice compared to wildtype (WT) littermates. Two-way ANOVA followed by Bonferroni's *posthoc* test; Mean ± SEM; Number of slips on a 28 mm round (E) and 10 mm square beam (F) of 7 week old NPC1$^{-/-}$ mice compared to WT littermates. Unpaired t-test; Mean + SEM; A−F: n = 12 per group; **p < 0.01; ***p < 0.001.

nesting behavior was observed from the eighth week onward, reaching the worst score at the age of 9 weeks (Fig. 1C).

To assess motor coordination, the Rota Rod and Beam Walk test were performed. NPC1$^{-/}$ mice showed a progressive decrease in the latency to fall off of the rod. When compared to WT littermates, significant differences were observed at 8−10 weeks of age (Fig. 1D).

The Beam Walk test was performed only with 7 week old animals since older animals are hardly able to stay on the beam. At this age, a significant difference in motor

https://doi.org/10.1016/j.heliyon.2019.e01293

coordination between NPC1$^{-/-}$ mice and WT littermates could be observed at each of the five beams used (Fig. 1E,F and data not shown). NPC1$^{-/-}$ mice presented a significantly increased number of slips compared to WT littermates. The highest amount of slips was observed on the square beam with 10 mm diameter, but even on the 28 mm round beam animals performed significantly worse than WT littermates (Fig. 1E and F).

2.2. Alterations in liver physiology of young NPC1$^{-/-}$ mice

At 6 weeks of age, the liver was weighed and the total levels of cholesterol and hepatic enzymes were measured in the liver and plasma, respectively. NPC1$^{-/-}$ mice showed a 1.2 fold increase in liver weight compared to WT littermates (Fig. 2A). Furthermore, total cholesterol levels were significantly higher in the liver of NPC1$^{-/-}$ mice compared to WT littermates (Fig. 2B).

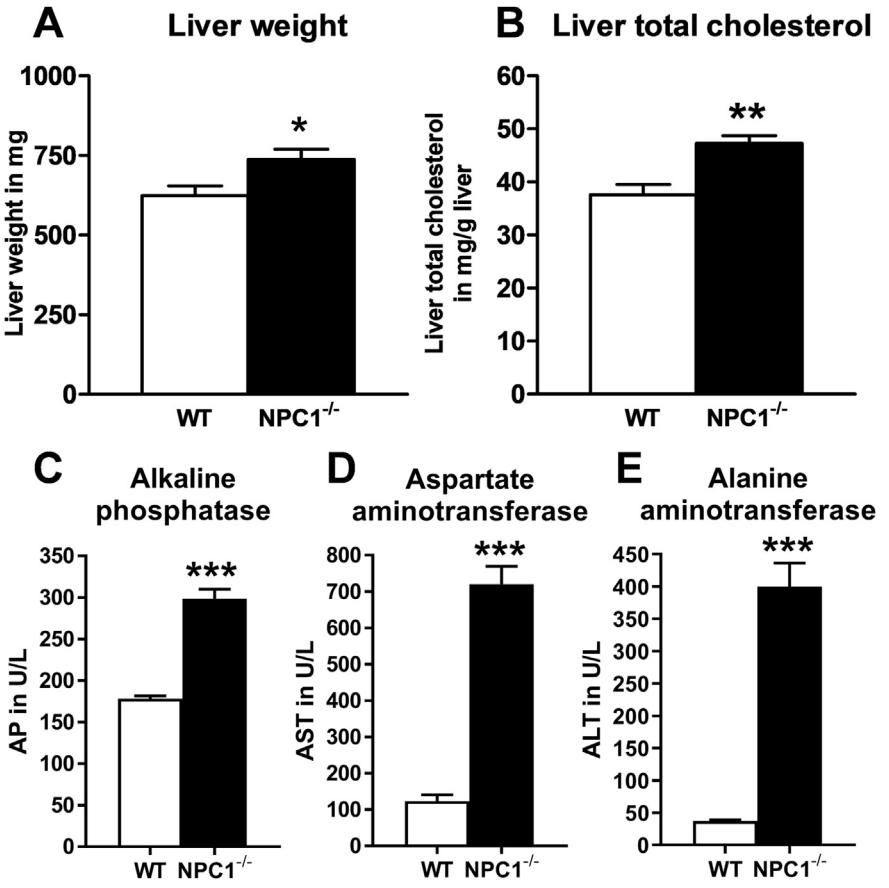

Fig. 2. Alterations in liver physiology of 6 week old NPC1$^{-/-}$ mice. Liver weight in milligram (A), total cholesterol levels in mg/g liver (B), alkaline phosphatase levels (AP; C), aspartate aminotransferase levels (AST; D) and alanine aminotransferase levels (ALT; E) in units per liter plasma of 6 week old NPC1$^{-/-}$ and WT littermates. Unpaired t-test; Mean + SEM; n = 6–8 per group; *p < 0.05; **p < 0.01; ***p < 0.001.

https://doi.org/10.1016/j.heliyon.2019.e01293

The levels of the three liver enzymes alkaline phosphatase (AP), aspartate aminotransferase (AST) and alanine aminotransferase (ALT) were significantly increased in NPC1$^{-/-}$ mice compared to WT littermates (Fig. 2C,D,E). The biggest difference was observed in ALT, showing an 8-fold increase in NPC1$^{-/-}$ mice compared to WT littermates (Fig. 2E).

2.3. Brain alterations of 6 week old NPC1$^{-/-}$ mice

In order to study possible brain alterations in NPC1$^{-/-}$ mice, the brain was weighed and the levels of total cholesterol and Aβ were measured in 6 week old mice compared to age-matched WT littermates. The weight of the cerebellum and cortex was significantly lower in NPC1$^{-/-}$ mice compared to WT littermates (Fig. 3A). The level of total cholesterol was assessed in different brain regions of NPC1$^{-/-}$ mice resulting in a significant decrease only in the hippocampus compared to WT littermates (Fig. 3B). Furthermore, Aβ levels were significantly increased in the hippocampus of NPC1$^{-/-}$ mice but not in the cerebellum or cortex (Fig. 3C).

2.4. Progressive neuroinflammation in NPC1$^{-/-}$ mice

Cytokine profiles were assessed in the cerebellum and hippocampus of 6 week old NPC1$^{-/-}$ and WT animals. IL-12p70 was significantly decreased in the cerebellum but increased in the hippocampus of NPC1$^{-/-}$ mice compared to WT littermates. Nevertheless, when data were analyzed by t-test, also IL-10 was significantly reduced while IL-1β and KC were significantly increased in the cerebellum of NPC1$^{-/-}$ mice compared to WT littermates (Fig. 4A, t-test significances not labeled). In the hippocampus, IFN-γ, KC and TNF-α were significantly increased in NPC1$^{-/-}$ mice compared to WT littermates when analyzed by t-test (Fig. 4B, t-test significances not labeled).

Quantitative immunofluorescence was used to evaluate neuroinflammation during disease progression. 4, 7 and 10 week old NPC1$^{-/-}$ and 10 week old WT animals were analyzed for GFAP and CD45 expression to visualize astrocytosis and activated microglia, respectively. In the cerebellum, 10 week old NPC1$^{-/-}$ mice showed higher, but not significant total GFAP signal than WT littermates of the same age. In NPC1$^{-/-}$ mice, the GFAP levels remained stable over time (Fig. 4C). Hippocampal GFAP levels did also not significantly change over age (Fig. 4D). CD45 labeling showed a significant increase of total signal over age in the hippocampus but not in the cerebellum of NPC1$^{-/-}$ animals ($p = 0.0568$; Fig. 4E,F).

Quantitative analysis of MAP2 total signal showed a slight decrease over age in NPC1$^{-/-}$ mice compared to WT littermates but data were not statistically significant (data not shown).

https://doi.org/10.1016/j.heliyon.2019.e01293

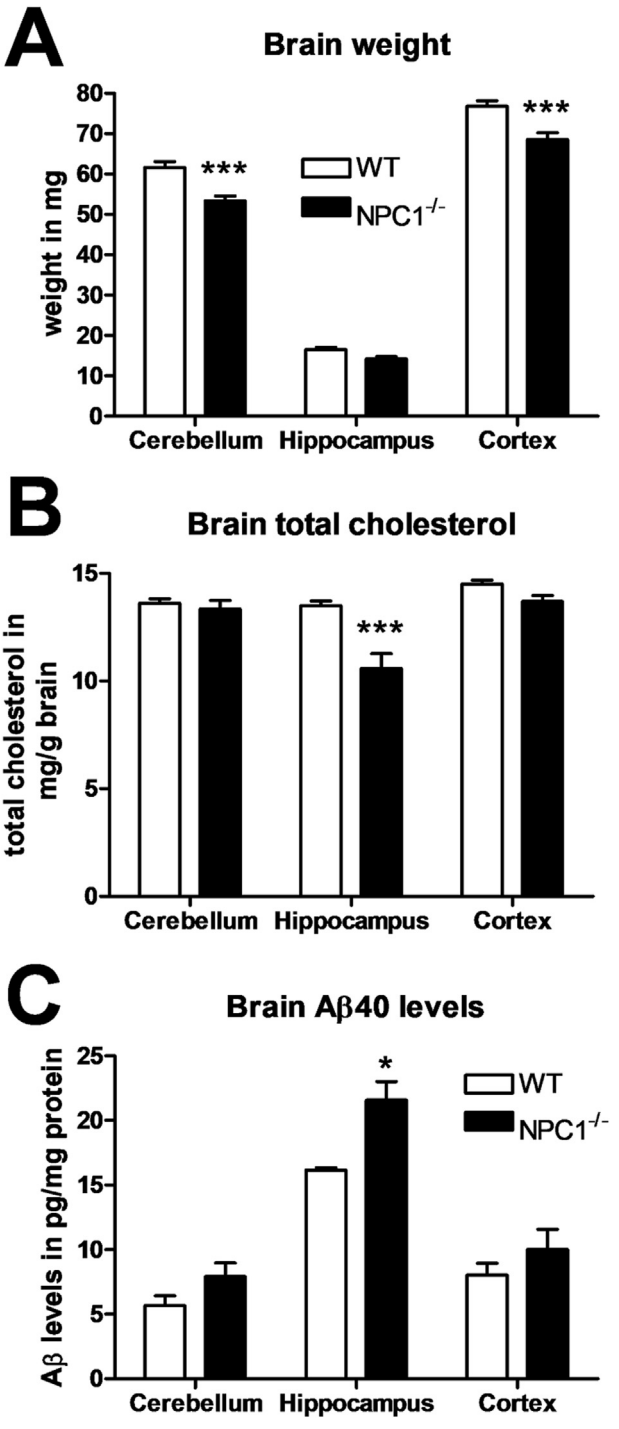

Fig. 3. Brain alterations of 6 week old NPC1$^{-/-}$ mice. Brain weight in milligram (A), total cholesterol levels in mg/g brain (B) and Aβ40 levels in pg/mg protein (C) in the cerebellum, hippocampus and cortex of 6 week old NPC1$^{-/-}$ and WT littermates. Two-way ANOVA followed by Bonferroni's *posthoc* test; n = 6 per group; Mean + SEM. *p < 0.05; ***p < 0.001.

https://doi.org/10.1016/j.heliyon.2019.e01293

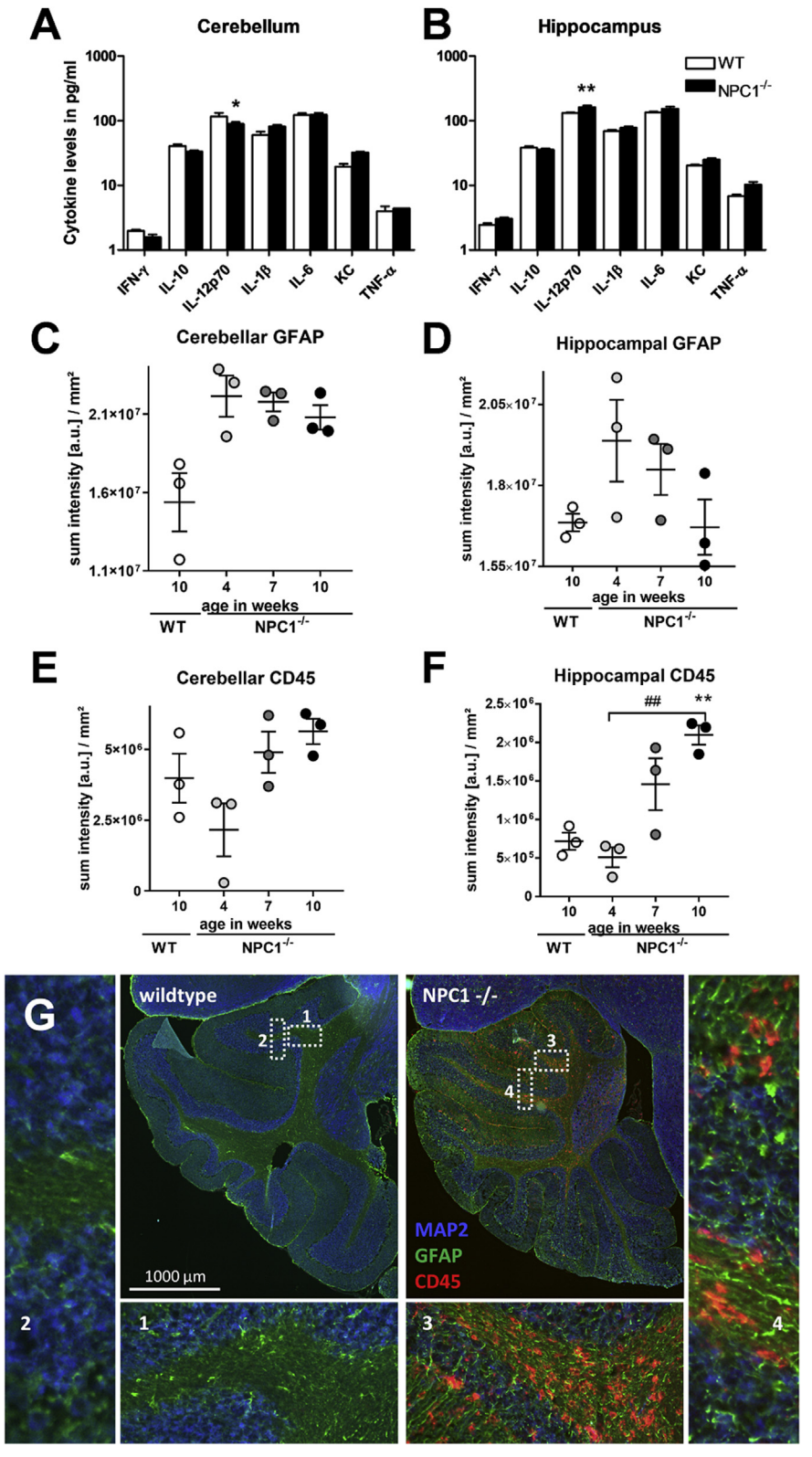

Fig. 4. Progressive neuroinflammation in NPC1$^{-/-}$ mice. Cerebellar (A) and hippocampal (B) cytokine profile of 6 week old NPC1$^{-/-}$ mice. Overall immunofluorescence signal of GFAP labelled astrocytes in

https://doi.org/10.1016/j.heliyon.2019.e01293

Representative images of the cerebellum show neuroinflammation observed as astrocyte reactivity by GFAP labeling and microglial activation by CD45 labeling (Fig. 4G).

2.5. Progressive cerebellar alterations of NPC1$^{-/-}$ mice

To evaluate the disease progression in adolescent NPC1$^{-/-}$ mice, 6 and 10 week old NPC1$^{-/-}$ and WT animals were analyzed. NPC1$^{-/-}$ mice showed a robust decreased cerebellar weight compared to WT mice at 10 weeks of age (Fig. 5A). The observed statistical significance in the cerebellum of 6 week old animals as shown in Fig. 3A could statistically not be verified in the here performed analysis as shown in Fig. 5A. Furthermore, cerebellar Aβ40 levels were increased in NPC1$^{-/-}$ animals compared to WT littermates at 10 weeks of age (Fig. 5B). Quantitative immunofluorescence was used to measure cerebellar pathology progression during adolescence. NPC1$^{-/-}$ mice were analyzed for Calbindin D-28k and APP expression at the age of 4, 7 and 10 weeks and compared to 10 week old WT littermates. Overall immunofluorescence signal of cerebellar Calbindin D-28k decreased over age resulting in significantly reduced Calbindin D-28k signal compared to WT littermates at the age of 10 weeks (Fig. 5C).

Cerebellar total APP signal was slightly but not significantly increased in NPC1$^{-/-}$ mice at the age of 10 weeks compared to 4 week old NPC1$^{-/-}$ mice suggesting a progressive increase of total APP in NPC1$^{-/-}$ mice ($p = 0.2214$). Total APP in 10 week old NPC1$^{-/-}$ mice was slightly decreased compared to 10 week old WT littermates ($p > 0.99$; Fig. 5D).

Representative images of the cerebellum show APP, Calbindin D-28k and DAPI labeling to visualize APP, Purkinje cell loss and nuclei for counterstaining (Fig. 5E).

In summary, our results demonstrate that NPC1$^{-/-}$ mice show diminished body weight and temperature in week 9 and 10, respectively. Furthermore, animals present robust motor deficits at 8 weeks of age. Already at the age of 6–7 weeks NPC1$^{-/-}$ mice also show an increased liver size and higher cholesterol and hepatic enzyme levels. The brain of NPC1$^{-/-}$ mice on the other hand presents a decreased weight compared to WT littermates and total cholesterol levels are diminished in the

the cerebellum (C) and hippocampus (D) of 4, 7 and 10 week old NPC1$^{-/-}$ mice and 10 week old WT littermates. Quantification of CD45 labelled microglia and leukocytes in the cerebellum (E) and hippocampus (F) of 4, 7 and 10 week old NPC1$^{-/-}$ mice and 10 week old control animals. A,B: n = 6, Two-way ANOVA followed by Bonferroni's *posthoc* test. Mean + SEM. C–F: n = 3, One-way ANOVA followed by Bonferroni's *posthoc* test. Mean ± SEM. *compared to WT; #changes over age; A–F: *$p < 0.05$; **$p < 0.01$. G: Representative images showing co-labeling of the cerebellum with GFAP + MAP2 + CD45, labelled astrocytes + principal neurons + microglia/leukocytes, respectively of 7 week old NPC1$^{-/-}$ and WT littermates. Scale bar: 1,000 μm.

https://doi.org/10.1016/j.heliyon.2019.e01293

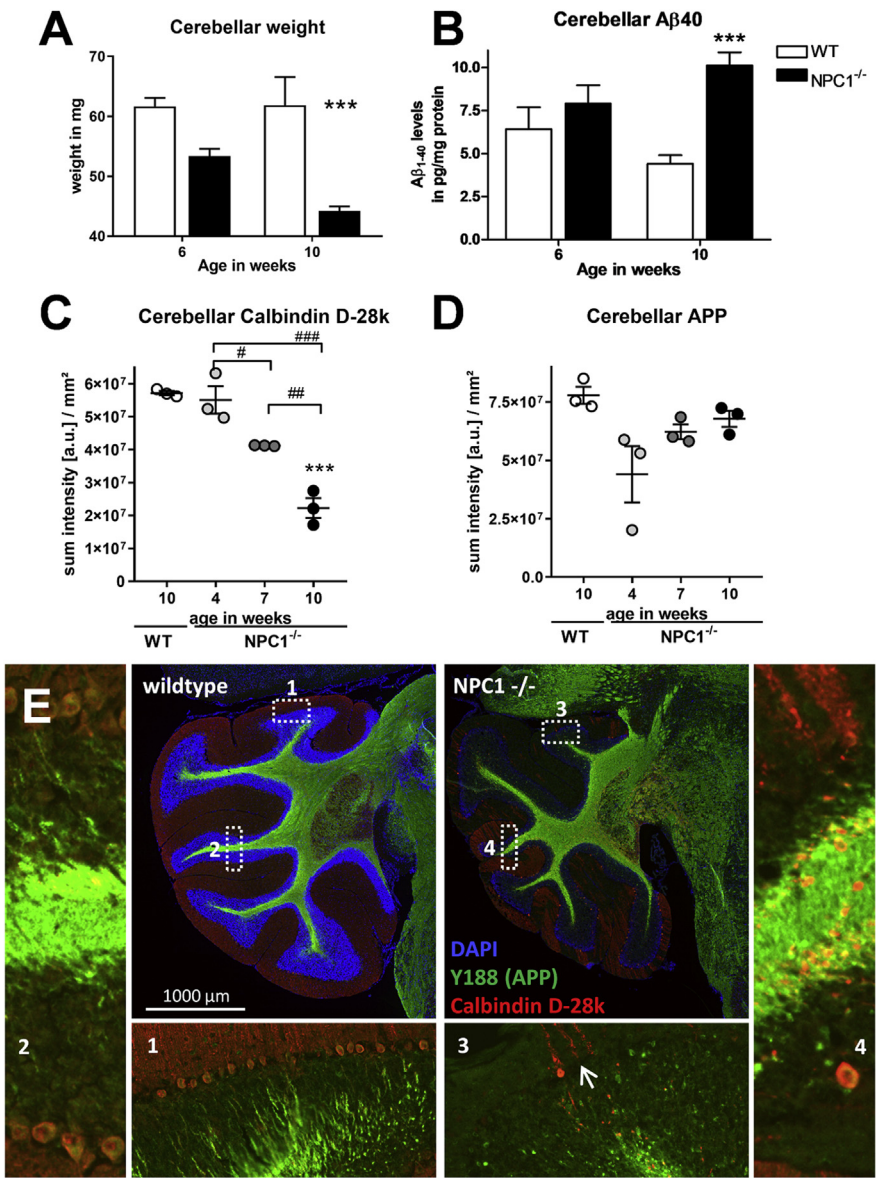

Fig. 5. Progressive cerebellar alterations of NPC1$^{-/-}$ mice. Cerebellar weight in milligram (A) and Aβ40 levels in pg/mg protein (B) in 6 and 10 week old NPC1$^{-/-}$ mice compared to age matched control animals. Overall immunofluorescence signal of cerebellar Calbindin D-28k (C) and APP (D) in 4, 7 and 10 week old NPC1$^{-/-}$ mice and 10 week old WT littermates. A,B: n = 6, Two-way ANOVA followed by Bonferroni's *posthoc* test. Mean + SEM. C,D: n = 3, One-way ANOVA followed by Bonferroni's *posthoc* test. Mean ± SEM. *compared to WT; #changes over age; A–D: *p < 0.05; **p < 0.01; ***p < 0.001. E: Representative images showing co-labeling of the cerebellum with Y188 + DAPI + Calbindin D-28k antibody labeling APP + nuclei + Purkinje cells, respectively of 7 week old NPC1$^{-/-}$ mice and WT littermates. Scale bar: 1,000 µm.

hippocampus. On the contrary, Aβ1-40, IL-12p70 and activated microglia levels are increased in that same brain region. The cerebellum is simultaneously characterized by highly increased astrocytosis, increased Aβ1-40 and decreasing Calbindin D-28k levels.

https://doi.org/10.1016/j.heliyon.2019.e01293

3. Discussion

In this study, we performed a behavioral and biochemical characterization of NPC1$^{-/-}$ mice to provide an overview of the hepatic and neuronal phenotype of NPC1$^{-/-}$ mice on a Balb/C background over age. The aim was to gain a better understanding of disease pathology and progression in this model in order to improve future therapeutic strategies.

Firstly, we focused on the general health and behavioral changes. Body weights were decreased at the age of 9 weeks compared to WT littermates. These results and the observed body weight curve over age is comparable with already published results and thus indicates a very robust and stable phenotype of NPC1$^{-/-}$ mice (Nicoli et al., 2016). Nest construction is widespread throughout the animal kingdom. For small rodents, nests are important for reproduction and shelter as well as for heat conservation, since rodents are very vulnerable to heat loss due to their small size. Nesting behavior has been shown to be sensitive to brain lesions, pharmacological agents and genetic mutations (Deacon, 2006). NPC1$^{-/-}$ mice showed a significantly decreased nesting behavior when compared to WT littermates at 8 weeks of age. These results show that NPC1$^{-/-}$ mice do have an impaired general health. Differences in nest building can be observed even before the onset of body weight loss and body temperature decrease and is thus a first indicator of disturbed wellbeing. Retaining the nest building activity requires sufficient motor skills for shredding the nest material. A decreased nest building activity can therefore depend on uncoordinated higher motor functions, or the motivation to organize the bedding into a nest structure for protection and warmth (Deacon, 2006; Lopez et al., 2011). Motor skills of NPC1$^{-/-}$ mice were hence analyzed next since NPC patients often present progressive functional limitations that may include difficulties with gait, balance and coordination (Sansare et al., 2018). In the Rota Rod test, NPC1$^{-/-}$ mice showed a progressive decrease in the latency to fall off the rod, which indicates a progressive increase of motor deficits. A robust phenotype in the Rota Rod test could be observed at the age of 8 weeks validating our previous analyses (Rabl et al., 2016). Analysis of NPC1$^{-/-}$ mice by other groups showed first motor deficits in the Rota Rod test already at the age of 7 weeks (Elrick et al., 2010; Hung et al., 2016). These differences might be caused by technical differences between the Rota Rod setups like speed or acceleration. In addition, the Beam Walk test showed an impaired motor behavior in NPC1$^{-/-}$ mice. Differences in this motor test could be observed earlier compared to the Rota Rod test, reflecting the higher sensitivity of the Beam Walk test. These results therefore validate that NPC1$^{-/-}$ mice show robust motor dysfunctions that can be evaluated by several commonly used motor tests.

Since the most common clinical visceral symptom of NPC is hepatosplenomegaly in combination with an altered metabolism of cholesterol and glycolipids in the liver (Elleder et al., 1984; Garver et al., 2007), these parameters were analyzed in

https://doi.org/10.1016/j.heliyon.2019.e01293

NPC1$^{-/-}$ mice. In the here presented data, the liver of NPC1$^{-/-}$ mice weighed significantly more and presented significantly increased cholesterol levels compared to WT littermates by the age of 6 weeks. Earlier analyses by others revealed an increase in liver weight as early as 4 weeks of age that starts to decrease with decreasing body weight at 8 weeks of age while cholesterol levels progressively increase over age (Miyawaki et al., 1983; Xie et al., 1999). Because NPC1$^{-/-}$ mice do not present the NPC1/2 transfer complex, the cells are unable to export the cholesterol from the late endosomes (Kwon et al., 2009), resulting in this observed phenotype. Plasma aspartate (AST), alanine aminotransferase (ALT) and alkaline phosphatase (AP) tests have become standards and are routinely used for diagnosis of liver diseases since all three enzymes are increased in most forms of liver injury (Williams and Hoofnagle, 1988). Consequently, the levels of the hepatic enzymes, AST, ALT and AP in the plasma of NPC1$^{-/-}$ mice are strongly increased at an age of 6 weeks validating results by Garver and colleagues (Garver et al., 2007), who state that the presence of liver damage is characterized by a significant increase in the concentration of ALT and AST in the plasma of NPC1$^{-/-}$ mice already at 5 weeks of age. These results could be confirmed by others (Beltroy et al., 2005, 2007). Since we observed a very strong increase in liver enzyme levels at the age of 6 weeks, the time differences between our results and Garver and colleagues, suggest a progressive increase of this pathological feature in NPC1$^{-/-}$ mice (Garver et al., 2007). Thus, we show that liver damage in NPC1$^{-/-}$ mice is a strong phenotype that can be evaluated by different markers. The observed hepatic pathology of NPC1$^{-/-}$ mice seems to be comparable with the pathology observed in NPC patients (vom Dahl and Mengel, 2010), suggesting a strong translational value of these alterations.

Since the disease is not only characterized by a visceral but also neuronal phenotype, the brain of NPC1$^{-/-}$ mice was analyzed next. Contrary to observations in the liver, the brain of 6 week old NPC1$^{-/-}$ mice weighed less compared to WT littermates. This is in accordance with results by Luan and coworkers, who already showed a diminished brain weight in 8 week old NPC1$^{-/-}$ mice (Luan et al., 2008). Xie and colleagues could even find first hints of a reduced brain weight in NPC1$^{-/-}$ mice at the age of 3 weeks (Xie et al., 1999). Reduced cerebellar weight was already shown to be related to a defective cerebellar granule cell proliferation (Nusca et al., 2014) but might also be related to the observed Purkinje cell loss in NPC1$^{-/-}$ mice. Purkinje cells are some of the largest neurons in the human brain exhibiting a dense dendritic synaptic network connecting with other cerebellar neurons (Tyrrell and Willshaw, 1992). Thus, it should be analyzed in more detail if the loss of Purkinje cells observed in NPC1$^{-/-}$ mice may lead to the loss of several of the connecting neurons, which would in turn lead to a strong decrease of the Purkinje cell layer and brain weight. Purkinje cell degeneration is indeed the most apparent cerebellar pathology in NPC1 animal models (Higashi et al., 1993; Sarna et al., 2003).

https://doi.org/10.1016/j.heliyon.2019.e01293

Moreover, cell specific deletion of the Npc1 gene in mature cerebellar Purkinje cells was shown to lead to an age-dependent Purkinje cell loss and impairments in motor skills (Elrick et al., 2010). Consequently, we assessed the levels of Calbindin D-28k, a marker of Purkinje cells and found a progressive decrease over age. This decline is significant at 7 weeks of age, the same age at which motor deficits are first observed. This is in agreement with published results by others that already showed a severe loss of Purkinje cells in NPC1$^{-/-}$ mice (Sarna et al., 2003; Kodam et al., 2010).

Some studies have shown that NPC disease exhibits some intriguing parallels with Alzheimer's disease (AD), the most common form of dementia. Among these characteristics are Aβ metabolism dysfunctions and paired helical filament tau aggregates (Auer et al., 1995; Mattsson et al., 2012). Our results show significantly higher hippocampal Aβ40 levels in 10 week old NPC1$^{-/-}$ mice, comparable to AD patients (Jimenez et al., 2014). Moreover, these results are in accordance with a study demonstrating a substantial accumulation of Aβ in neurons with NPC defect (Jin et al., 2004).

Since amyloid-β results from processing of APP also the levels of total Amyloid Precursor Protein (APP) in the brain were measured. Multiple studies showed evidence of an increase of APP products such as Aβ40, Aβ42 and the C-terminal end in the hippocampus of NPC1$^{-/-}$ mice (Jin et al., 2004; Kodam et al., 2010; Yanez et al., 2016). Analyzing total cerebellar APP levels showed a progressive increase of APP over age in NPC1$^{-/-}$ mice. This increase could be related to the increase of Aβ40 observed in our study and the fact that redistribution of cholesterol in the NPC1 deficient mouse brain is associated with increased processing of APP (Kodam et al., 2010).

Additionally, inflammation was analyzed in the brain showing reduced cerebellar IL-12p70 levels in 6 week old NPC1$^{-/-}$ mice, confirming the observation in NPC patients showing significantly decreased IL-12p70 levels in the CSF fluid (Cologna et al., 2014). Furthermore, we show significantly higher hippocampal IL-12p70 levels in 6 week old NPC1$^{-/-}$ mice that are hence contradicting results in NPC patients. Our analyses of further cytokines did not result in any significant changes in NPC1$^{-/-}$ mice although Cologna and colleagues already showed increased cytokine levels by qPCR analyses as early as 3 weeks of age. Differences in IL1β levels between these studies might be caused by different analyses methods since Cologna used qPCR measurement of mRNA while we analyzed actual protein levels. Additional markers analyzed by Cologna and coworkers include Ccl3/Mip1a, Ccl8, C3, Cxcl9 and Cxcl10 and therefore differ from cytokines analyzed in the here presented study (Cologna et al., 2014).

Furthermore, inflammation is a feature that is shared by most neurodegenerative diseases (reviewed by (Chen et al., 2016)). Interleukin 12 (IL-12) is an inflammatory cytokine that promotes the response of the immune system (Murphy et al., 1994;

https://doi.org/10.1016/j.heliyon.2019.e01293

Table 1. Summary of robust behavioral and hepatic phenotype presence in NPC1$^{-/-}$ mice.

		Age in weeks	Effect
Health and Behavior	Body Weight	9	↓
	Body Temperature	10	↓
	Nest Building	8	↓
	Rota Rod	8	↓
	Beam Walk	7	↓
Liver	Liver weight	6	↑
	Total cholesterol	6	↑
	Alkaline Phosphatase	6	↑
	Aspartate Aminotransferase	6	↑
	Alanine Aminotransferase	6	↑

Overview of general health and behavioral changes as well as pathologies observed in the liver of NPC1$^{-/-}$ mice. Please be aware that 'age in weeks' is defined as the time when pathology is robust. This time is usually later than the age of pathology onset. ↑: increase; ↓: decrease.

Table 2. Summary of robust neuronal phenotype presence in NPC1$^{-/-}$ mice.

	Cerebellum		Hippocampus		Cortex	
	Age in weeks	Effect	Age in weeks	Effect	Age in weeks	Effect
Weight	10	↓	6	–	6	↓
Total cholesterol	6	–	6	↓	6	–
Abeta 40 levels	10	↑	6	↑	6	–
APP	10	–	N/A	N/A	N/A	N/A
IL-12p70	6	↓	6	↑	N/A	N/A
Astrocytosis	4	↑ (n.s.)	10	–	N/A	N/A
Activated Microglia	10	–	10	↑	N/A	N/A
Calbindin D-28k	10	↓	N/A	N/A	N/A	N/A
MAP2	10	–	10	–	N/A	N/A

Overview of pathologies observed in the cerebellum, hippocampus and cortex of NPC1$^{-/-}$ mice. Please be aware that 'age in weeks' is defined as the time when pathology is robust. This time is usually later than the age of pathology onset. -: no changes observed; ↑: increase; ↓: decrease; n.s.: not significant; N/A: not analyzed.

Table 3. List of primary antibodies used for histological evaluations.

Primary antibodies

Species	Antigen	Clone	Source	Dilution
rabbit	GFAP	poly	Dako	1:500
mouse	MAP2	SMI-52	BioLegend	1:2000
rat	CD45	30-F11	abcam	1:800
mouse	Calbindin D-28k	300	Swant	1:2000
rabbit	APP	Y188	abcam	1:500

https://doi.org/10.1016/j.heliyon.2019.e01293

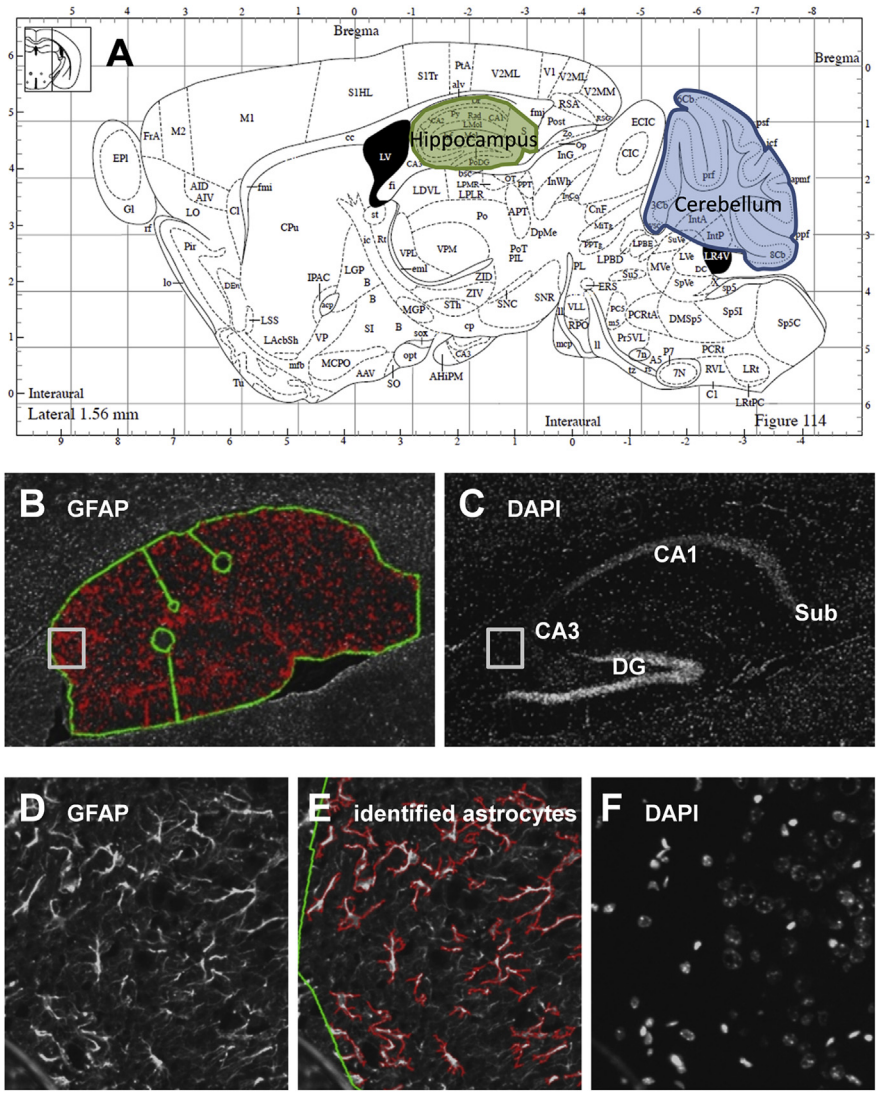

Fig. 6. Definition of AOI and quantitative image analysis. (A) The areas of interest (AOI) outline the entire hippocampal formation and the cerebellum. (B) Example of an AOI (green line) drawn manually on an image of a GFAP-labelled section using the drawing function in Image Pro Plus 6.2; note that artifacts such as air bubbles were excluded. Identified GFAP-immunoreactive cells are indicated in red. (C) DAPI labeling on the same section as shown in B. (D) Higher magnification showing immunofluorescent labeling of GFAP in hippocampal CA3 region. (E) Same image as D with a red overlay surrounding identified astrocytes. Filter parameters were as follows: 8 bit minimum intensity threshold: 72; minimum object size: 30 μm^2. Note that the filter parameters were defined restrictively to minimize inclusion of false positive objects. (F) DAPI labeling on the same region as shown in D and E.

Hsieh et al., 2008). In AD, where Aβ levels are increased, an increase of IL-12 can be observed (Hussien et al., 2018). Here we show significantly higher hippocampal IL-12p70 levels in NPC1$^{-/-}$ mice at 6 weeks of age. Since the accumulation of Aβ40 is not significant until 10 weeks, it seems plausible that inflammation precedes and worsens the pathology of Aβ40 in NPC disease.

https://doi.org/10.1016/j.heliyon.2019.e01293

As already mentioned, NPC shares some characteristics with AD, including gliosis. Therefore, we studied GFAP, a glial protein expressed in mature astrocytes, in the NPC1$^{-/-}$ mouse brain. GFAP is considered a marker for astrocytosis, and known to be induced upon brain damage or during CNS degeneration (for review see (Middeldorp and Hol, 2011)). In 4 week old NPC1$^{-/-}$ mice the number of reactive astrocytes was already as high as in 10 week old NPC1$^{-/-}$ mice thus presenting a similar onset of astrocytosis as already shown by Baudry and co-workers, who showed first signs of astrocytosis as early as 2 weeks of age with a strong increase in the following two weeks of age (Baudry et al., 2003). Increased reactive astrocytes have also been demonstrated in human *post-mortem* brain of NPC patients (Chiba et al., 2014; Cologna et al., 2014), making this pathology relevant for translational NPC1 research. In order to determine whether NPC1$^{-/-}$ mice show microgliosis, CD45 was examined, an enzyme expressed in microglial cells during CNS inflammation (Ponomarev et al., 2005). Our results show a progressive increase of CD45 signal in NPC1$^{-/-}$ mice. Summarizing, these results suggest that NPC1 knock out causes neuroinflammation with a robust phenotype presence already at 4 weeks of age. A summary of results giving the age of robust phenotype presence is listed in Tables 1 and 2.

4. Conclusions

In summary, this study confirms an early start of the phenotype in NPC1$^{-/-}$ mice. Robust early pathological changes observed in the mouse model are neuroinflammation in the cerebellum as well as loss of brain weight and increase of Aβ in the hippocampus. Furthermore, we have also shown that loss of Purkinje cells occurs slightly earlier than motor deficits. Additionally, for the first time a decrease in hippocampal cholesterol levels is demonstrated that is paralleled by severely increased hepatic cholesterol levels. The hepatic and neuronal phenotype is succeeded by general health and motor deficits. Taken together, our results validate already published results, verify the stability of the mice's phenotype, pinpoint the age of robust phenotype presence and thus reinforce the use of these animals to study NPC disease and its possible therapies.

5. Materials and methods

5.1. Animals

All animals were bred and housed under identical conditions in individually ventilated cages on standardized rodent bedding (Rettenmayer®) in the AAALAC accredited animal facility of QPS Austria GmbH. Cotton nestlets (Plexx®) were provided as nesting material. The room temperature was kept at approximately 21 °C and the relative humidity between 40-70%. Mice were housed under

https://doi.org/10.1016/j.heliyon.2019.e01293

constant light-cycle (12 hours light/dark). Dried pelleted standard rodent chow (Altromin®) and normal tap water were available to the animals *ad libitum*. Each individual animal was checked regularly for any clinical sign. Male and female animals of equal number were used. Mice were housed in same sex groups of up to four animals. During weaning, less than 1 mm of the tail tip was taken from each animal and used for genotyping. Actual animal numbers are given in the figure legends. All efforts were made to minimize suffering. Heterozygous $NPC1^{+/-}$ mice [BALB/cNctr-Npc1<m1N>/J (Jackson Laboratories # 003092)] were mated and resulting homozygous $NPC1^{-/-}$ and wildtype $NPC1^{+/+}$ mice used for experiments.

5.2. Ethics approval and consent to participate

Animal studies conformed to the Austrian guidelines for the care and use of laboratory animals and were approved by the Styrian government, Austria (ABT13-78Jo-109-2012-1).

5.3. Behavioral tests

All behavioral tests were performed during the early phase of the light cycle. Before the start of each behavioral test, animals were habituated to the experimental room for at least 1 hour. Animals were tested in the Rota Rod test and Nest Building Test starting at the age of 5 weeks until 10 weeks of age when animals showed strongest deficits in the motor tests. Beam Walk test was performed at an age of 7 weeks. Animals were allocated to the corresponding experimental group according to their genotype. The body weight was measured using a standard precision scale. The body temperature was measured with a rectal thermometer. The Rota Rod test, Beam walk test and Nest building test were performed as previously described (Rabl et al., 2016, 2017).

5.4. Tissue sampling

All mice were anesthetized by an overdose of the inhalation anesthesia isofluran. Once animals were deeply anesthetized, the thorax was opened and blood was drawn by heart puncture of the left ventricle and collected in lithium heparin tubes. Mice were afterwards transcardially perfused with physiological (0.9%) saline. Thereafter, liver and brain were taken, brain hemisected and all tissues weight using a precision scale. The right brain hemisphere was fixed by immersion at 4 °C in freshly prepared 4% formaldehyde in phosphate buffer (pH 7.4) for 24 hours. After cryo-conservation in a 15% sucrose/phosphate buffered saline (PBS) solution, tissues were shock frozen in dry-ice cooled liquid isopentane and stored at -80 °C until used for histological analyses. The left brain hemisphere was

https://doi.org/10.1016/j.heliyon.2019.e01293

further dissected in hippocampus, cortex, cerebellum and remaining brain and all brain parts and the liver immediately shock frozen on dry ice and stored at -80 °C until used for biochemical analyses.

5.5. Plasma preparation

The blood was centrifuged at 1,000 x g for 10 min at room temperature (RT) and plasma transferred to fresh tubes, frozen on dry ice and stored at -80 °C until used for analyses.

5.6. Measurement of total cholesterol levels

Liver and brain regions were homogenized with 20% w/v homogenization buffer (20 mM Tris-HCl, pH 7.4, 150 mM NaCl, 1 mM EDTA, 1% Nonidet P-40, 1% Triton X-100, 2% SDS, and protease and phosphatase inhibitors). For the release of total cholesterol the homogenates were mixed 1:1 with extraction buffer (20 mM Tris-HCl, pH 7.4, including 15% Brij 35 and 1% methyl-β-cyclodextrin) (Kirsch et al., 2002). After 60 min of incubation on a plate shaker, samples were analyzed for total cholesterol levels using the colorimetric assay Fluitest-CHOL (Analyticon, #4241; Lichtenfels, Germany).

5.7. Measurement of liver enzymes in plasma

Liver enzymes aspartate aminotransferase (AST), alanine aminotransferase (ALT) and alkaline phosphatase (AP) were analyzed in lithium-heparin plasma samples using the colorimetric assays Fluitest- GOT ASAT, Fluitest- GPT ALAT and Fluitest-AP (Analyticon, #1177; #1187; #1186; Lichtenfels, Germany), respectively.

5.8. Measurement of Aβ40 and cytokines

Samples were analyzed for Aβ40 levels using the MSD® 96-well Human (6E10) Aβ40 Ultra-Sensitive Kit (#K151FTE-1; Mesoscale Discovery, Rockville, USA) and for cytokine levels using the MSD® 96-well V-PLEX Proinflammatory Panel 1 Mouse Kit (#K15048D; Mesoscale Discovery, Rockville, USA). Both immunosorent assays were performed according the manufacturer's protocol.

5.9. Histology

Frozen brain hemispheres were cut sagittally on a cryostat (Leica CM3050S). Unless indicated otherwise, a systematic uniform random set of five mounted 10 μm thick brain sections from five medio-lateral levels per animal were used for immunofluorescent labeling.

https://doi.org/10.1016/j.heliyon.2019.e01293

GFAP + CD45 + MAP2 and Calbindin D-28k + APP incubation of brain sections were conducted as previously described (Rabl et al., 2017). A list of primary antibodies used for histological labeling is shown in Table 3.

Whole slide mosaic images of labelled sections were recorded on a fully motorized Zeiss AxioImager Z1 microscope with 10x high aperture lens, equipped with a Zeiss AxioCam MRm camera and ZEN 2.3 software. Mosaic images were merged and converted to full resolution single channel tif files that were used for quantitative image analysis (Fig. 6). The target area was identified by drawing an area of interest (AOI) on the images. Background correction was used if necessary, and imunofluorescence signals were then quantified by adequate thresholding and morphological filtering (size, shape) to determine the normalized accumulated brightness of all pixels on identified immunopositive objects [signal intensity/mm^2]. Once the parameters of the targeted objects had been defined in a test run, the quantitative image analysis ran automatically by a macro so that the results are rater-independent and fully reproducible from the raw images. All measurements were performed using Image Pro Plus (v6.2) software.

5.10. Statistics

Data analysis was performed in GraphPad Prism™ 4.03 (GraphPad Software Inc., USA). Graphs show group means and standard error of the mean (SEM). The significance level was set at $p < 0.05$. Group means were compared using unpaired t-test or Two-way analysis of variance (ANOVA) with a subsequent *post-hoc* test. The utilized statistical tests and exact sample numbers are mentioned in the figure legends.

Declarations

Author contribution statement

Estibaliz Santiago-Mujica: Performed the experiments; Analyzed and interpreted the data; Wrote the paper.

Stefanie Flunkert: Conceived and designed the experiments; Analyzed and interpreted the data; Wrote the paper.

Roland Rabl, Joerg Neddens, Tina Loeffler: Conceived and designed the experiments; Performed the experiments; Analyzed and interpreted the data.

Birgit Hutter-Paier: Conceived and designed the experiments; Contributed reagents, materials, analysis tools or data

Funding statement

This work was funded by R&D budget of QPS Austria GmbH.

https://doi.org/10.1016/j.heliyon.2019.e01293

Competing interest statement

The authors declare the following conflict of interests: All authors are or were employees of QPS Austria GmbH.

Additional information

No additional information is available for this paper.

Acknowledgements

We greatly thank Irene Schilcher and the whole research team of QPS Austria GmbH for proof reading and their technical support.

References

Amigo, L., Mendoza, H., Castro, J., Quinones, V., Miquel, J.F., Zanlungo, S., 2002. Relevance of Niemann-Pick type C1 protein expression in controlling plasma cholesterol and biliary lipid secretion in mice. Hepatology 36, 819–828.

Auer, I.A., Schmidt, M.L., Lee, V.M., Curry, B., Suzuki, K., Shin, R.W., Pentchev, P.G., Carstea, E.D., Trojanowski, J.Q., 1995. Paired helical filament tau (PHFtau) in Niemann-Pick type C disease is similar to PHFtau in Alzheimer's disease. Acta Neuropathol. 90, 547–551.

Baudry, M., Yao, Y., Simmons, D., Liu, J., Bi, X., 2003. Postnatal development of inflammation in a murine model of Niemann-Pick type C disease: immunohistochemical observations of microglia and astroglia. Exp. Neurol. 184, 887–903.

Beltroy, E.P., Liu, B., Dietschy, J.M., Turley, S.D., 2007. Lysosomal unesterified cholesterol content correlates with liver cell death in murine Niemann-Pick type C disease. J. Lipid Res. 48, 869–881.

Beltroy, E.P., Richardson, J.A., Horton, J.D., Turley, S.D., Dietschy, J.M., 2005. Cholesterol accumulation and liver cell death in mice with Niemann-Pick type C disease. Hepatology 42, 886–893.

Bowman, E.A., Velakoulis, D., Desmond, P., Walterfang, M., 2018. Longitudinal changes in white matter fractional anisotropy in adult-onset niemann-pick disease type C patients treated with miglustat. JIMD Rep. 39, 39–43.

Bowman, E.A., Walterfang, M., Abel, L., Desmond, P., Fahey, M., Velakoulis, D., 2015. Longitudinal changes in cerebellar and subcortical volumes in adult-onset Niemann-Pick disease type C patients treated with miglustat. J. Neurol. 262, 2106–2114.

 https://doi.org/10.1016/j.heliyon.2019.e01293

Carstea, E.D., Morris, J.A., Coleman, K.G., Loftus, S.K., Zhang, D., Cummings, C., Gu, J., Rosenfeld, M.A., Pavan, W.J., Krizman, D.B., Nagle, J., Polymeropoulos, M.H., Sturley, S.L., Ioannou, Y.A., Higgins, M.E., Comly, M., Cooney, A., Brown, A., Kaneski, C.R., Blanchette-Mackie, E.J., Dwyer, N.K., Neufeld, E.B., Chang, T.Y., Liscum, L., Strauss 3rd, J.F., Ohno, K., Zeigler, M., Carmi, R., Sokol, J., Markie, D., O'Neill, R.R., van Diggelen, O.P., Elleder, M., Patterson, M.C., Brady, R.O., Vanier, M.T., Pentchev, P.G., Tagle, D.A., 1997. Niemann-Pick C1 disease gene: homology to mediators of cholesterol homeostasis. Science 277, 228−231.

Chen, W.W., Zhang, X., Huang, W.J., 2016. Role of neuroinflammation in neurodegenerative diseases (Review). Mol. Med. Rep. 13, 3391−3396.

Chiba, Y., Komori, H., Takei, S., Hasegawa-Ishii, S., Kawamura, N., Adachi, K., Nanba, E., Hosokawa, M., Enokido, Y., Kouchi, Z., Yoshida, F., Shimada, A., 2014. Niemann-Pick disease type C1 predominantly involving the frontotemporal region, with cortical and brainstem Lewy bodies: an autopsy case. Neuropathology 34, 49−57.

Cologna, S.M., Cluzeau, C.V., Yanjanin, N.M., Blank, P.S., Dail, M.K., Siebel, S., Toth, C.L., Wassif, C.A., Lieberman, A.P., Porter, F.D., 2014. Human and mouse neuroinflammation markers in Niemann-Pick disease, type C1. J. Inherit. Metab. Dis. 37, 83−92.

Deacon, R.M., 2006. Assessing nest building in mice. Nat. Protoc. 1, 1117−1119.

Elleder, M., Smid, F., Hyniova, H., Cihula, J., Zeman, J., Macek, M., 1984. Liver findings in Niemann-Pick disease type C. Histochem. J. 16, 1147−1170.

Elrick, M.J., Pacheco, C.D., Yu, T., Dadgar, N., Shakkottai, V.G., Ware, C., Paulson, H.L., Lieberman, A.P., 2010. Conditional Niemann-Pick C mice demonstrate cell autonomous Purkinje cell neurodegeneration. Hum. Mol. Genet. 19, 837−847.

Garver, W.S., Jelinek, D., Oyarzo, J.N., Flynn, J., Zuckerman, M., Krishnan, K., Chung, B.H., Heidenreich, R.A., 2007. Characterization of liver disease and lipid metabolism in the Niemann-Pick C1 mouse. J. Cell. Biochem. 101, 498−516.

Group, N.-C.G.W., Wraith, J.E., Baumgartner, M.R., Bembi, B., Covanis, A., Levade, T., Mengel, E., Pineda, M., Sedel, F., Topcu, M., Vanier, M.T., Widner, H., Wijburg, F.A., Patterson, M.C., 2009. Recommendations on the diagnosis and management of Niemann-Pick disease type C. Mol. Genet. Metabol. 98, 152−165.

Higashi, Y., Murayama, S., Pentchev, P.G., Suzuki, K., 1993. Cerebellar degeneration in the Niemann-Pick type C mouse. Acta Neuropathol. 85, 175−184.

https://doi.org/10.1016/j.heliyon.2019.e01293

Hsieh, C.S., Macatonia, S.E., Tripp, C.S., Wolf, S.F., O'Garra, A., Murphy, K.M., 2008. Pillars article: development of TH1 CD4+ T cells through IL-12 produced by Listeria-induced macrophages. 1993. Science 260(5107): 547-549. J. Immunol. 181, 4437−4439.

Hung, Y.H., Walterfang, M., Churilov, L., Bray, L., Jacobson, L.H., Barnham, K.J., Jones, N.C., O'Brien, T.J., Velakoulis, D., Bush, A.I., 2016. Neurological dysfunction in early maturity of a model for niemann-pick C1 carrier status. Neurotherapeutics 13, 614−622.

Hussien, H.M., Abd-Elmegied, A., Ghareeb, D.A., Hafez, H.S., Ahmed, H.E.A., El-Moneam, N.A., 2018. Neuroprotective effect of berberine against environmental heavy metals-induced neurotoxicity and Alzheimer's-like disease in rats. Food Chem. Toxicol. 111, 432−444.

Jimenez, S., Navarro, V., Moyano, J., Sanchez-Mico, M., Torres, M., Davila, J.C., Vizuete, M., Gutierrez, A., Vitorica, J., 2014. Disruption of amyloid plaques integrity affects the soluble oligomers content from Alzheimer disease brains. PLoS One 9, e114041.

Jin, L.W., Shie, F.S., Maezawa, I., Vincent, I., Bird, T., 2004. Intracellular accumulation of amyloidogenic fragments of amyloid-beta precursor protein in neurons with Niemann-Pick type C defects is associated with endosomal abnormalities. Am. J. Pathol. 164, 975−985.

Kirsch, C., Eckert, G.P., Mueller, W.E., 2002. Cholesterol attenuates the membrane perturbing properties of beta-amyloid peptides. Amyloid 9, 149−159.

Kodam, A., Maulik, M., Peake, K., Amritraj, A., Vetrivel, K.S., Thinakaran, G., Vance, J.E., Kar, S., 2010. Altered levels and distribution of amyloid precursor protein and its processing enzymes in Niemann-Pick type C1-deficient mouse brains. Glia 58, 1267−1281.

Kulinski, A., Vance, J.E., 2007. Lipid homeostasis and lipoprotein secretion in Niemann-Pick C1-deficient hepatocytes. J. Biol. Chem. 282, 1627−1637.

Kwon, H.J., Abi-Mosleh, L., Wang, M.L., Deisenhofer, J., Goldstein, J.L., Brown, M.S., Infante, R.E., 2009. Structure of N-terminal domain of NPC1 reveals distinct subdomains for binding and transfer of cholesterol. Cell 137, 1213−1224.

Li, H., Repa, J.J., Valasek, M.A., Beltroy, E.P., Turley, S.D., German, D.C., Dietschy, J.M., 2005. Molecular, anatomical, and biochemical events associated with neurodegeneration in mice with Niemann-Pick type C disease. J. Neuropathol. Exp. Neurol. 64, 323−333.

https://doi.org/10.1016/j.heliyon.2019.e01293

Lloyd-Evans, E., Platt, F.M., 2010. Lipids on trial: the search for the offending metabolite in Niemann-Pick type C disease. Traffic 11, 419–428.

Loftus, S.K., Morris, J.A., Carstea, E.D., Gu, J.Z., Cummings, C., Brown, A., Ellison, J., Ohno, K., Rosenfeld, M.A., Tagle, D.A., Pentchev, P.G., Pavan, W.J., 1997. Murine model of Niemann-Pick C disease: mutation in a cholesterol homeostasis gene. Science 277, 232–235.

Lopez, M.E., Klein, A.D., Dimbil, U.J., Scott, M.P., 2011. Anatomically defined neuron-based rescue of neurodegenerative Niemann-Pick type C disorder. J. Neurosci. 31, 4367–4378.

Luan, Z., Saito, Y., Miyata, H., Ohama, E., Ninomiya, H., Ohno, K., 2008. Brainstem neuropathology in a mouse model of Niemann-Pick disease type C. J. Neurol. Sci. 268, 108–116.

Lyseng-Williamson, K.A., 2014. Miglustat: a review of its use in Niemann-Pick disease type C. Drugs 74, 61–74.

Mattsson, N., Olsson, M., Gustavsson, M.K., Kosicek, M., Malnar, M., Mansson, J.E., Blomqvist, M., Gobom, J., Andreasson, U., Brinkmalm, G., Vite, C., Hecimovic, S., Hastings, C., Blennow, K., Zetterberg, H., Portelius, E., 2012. Amyloid-beta metabolism in Niemann-Pick C disease models and patients. Metab. Brain Dis. 27, 573–585.

Mengel, E., Klunemann, H.H., Lourenco, C.M., Hendriksz, C.J., Sedel, F., Walterfang, M., Kolb, S.A., 2013. Niemann-Pick disease type C symptomatology: an expert-based clinical description. Orphanet J. Rare Dis. 8, 166.

Middeldorp, J., Hol, E.M., 2011. GFAP in health and disease. Prog. Neurobiol. 93, 421–443.

Miyawaki, S., Mitsuoka, S., Sakiyama, T., Kitagawa, T., 1983. Time course of hepatic lipids accumulation in a strain of mice with an inherited deficiency of sphingomyelinase. J. Hered. 74, 465–468.

Murphy, E.E., Terres, G., Macatonia, S.E., Hsieh, C.S., Mattson, J., Lanier, L., Wysocka, M., Trinchieri, G., Murphy, K., O'Garra, A., 1994. B7 and interleukin 12 cooperate for proliferation and interferon gamma production by mouse T helper clones that are unresponsive to B7 costimulation. J. Exp. Med. 180, 223–231.

Nicoli, E.R., Al Eisa, N., Cluzeau, C.V., Wassif, C.A., Gray, J., Burkert, K.R., Smith, D.A., Morris, L., Cologna, S.M., Peer, C.J., Sissung, T.M., Uscatu, C.D., Figg, W.D., Pavan, W.J., Vite, C.H., Porter, F.D., Platt, F.M., 2016. Defective

https://doi.org/10.1016/j.heliyon.2019.e01293

cytochrome P450-catalysed drug metabolism in niemann-pick type C disease. PLoS One 11, e0152007.

Nusca, S., Canterini, S., Palladino, G., Bruno, F., Mangia, F., Erickson, R.P., Fiorenza, M.T., 2014. A marked paucity of granule cells in the developing cerebellum of the Npc1(-/-) mouse is corrected by a single injection of hydroxypropyl-beta-cyclodextrin. Neurobiol. Dis. 70, 117−126.

Ong, W.Y., Kumar, U., Switzer, R.C., Sidhu, A., Suresh, G., Hu, C.Y., Patel, S.C., 2001. Neurodegeneration in Niemann-Pick type C disease mice. Exp. Brain Res. 141, 218−231.

Paul, C.A., Boegle, A.K., Maue, R.A., 2004. Before the loss: neuronal dysfunction in Niemann-Pick Type C disease. Biochim. Biophys. Acta 1685, 63−76.

Pentchev, P.G., Gal, A.E., Booth, A.D., Omodeo-Sale, F., Fouks, J., Neumeyer, B.A., Quirk, J.M., Dawson, G., Brady, R.O., 1980. A lysosomal storage disorder in mice characterized by a dual deficiency of sphingomyelinase and glucocerebrosidase. Biochim. Biophys. Acta 619, 669−679.

Ponomarev, E.D., Shriver, L.P., Maresz, K., Dittel, B.N., 2005. Microglial cell activation and proliferation precedes the onset of CNS autoimmunity. J. Neurosci. Res. 81, 374−389.

Rabl, R., Breitschaedel, C., Flunkert, S., Duller, S., Amschl, D., Neddens, J., Niederkofler, V., Rockenstein, E., Masliah, E., Roemer, H., Hutter-Paier, B., 2017. Early start of progressive motor deficits in Line 61 alpha-synuclein transgenic mice. BMC Neurosci. 18, 22.

Rabl, R., Horvath, A., Breitschaedel, C., Flunkert, S., Roemer, H., Hutter-Paier, B., 2016. Quantitative evaluation of orofacial motor function in mice: the pasta gnawing test, a voluntary and stress-free behavior test. J. Neurosci. Methods 274, 125−130.

Sansare, A., Zampieri, C., Alter, K., Stanley, C., Farhat, N., Keener, L.A., Porter, F., 2018. Gait, balance, and coordination impairments in Niemann pick disease, type C1. J. Child Neurol. 33, 114−124.

Sarna, J.R., Larouche, M., Marzban, H., Sillitoe, R.V., Rancourt, D.E., Hawkes, R., 2003. Patterned Purkinje cell degeneration in mouse models of Niemann-Pick type C disease. J. Comp. Neurol. 456, 279−291.

Sedel, F., Chabrol, B., Audoin, B., Kaphan, E., Tranchant, C., Burzykowski, T., Tourbah, A., Vanier, M.T., Galanaud, D., 2016. Normalisation of brain spectroscopy findings in Niemann-Pick disease type C patients treated with miglustat. J. Neurol. 263, 927−936.

https://doi.org/10.1016/j.heliyon.2019.e01293

Smith, D., Wallom, K.L., Williams, I.M., Jeyakumar, M., Platt, F.M., 2009. Beneficial effects of anti-inflammatory therapy in a mouse model of Niemann-Pick disease type C1. Neurobiol. Dis. 36, 242–251.

Tyrrell, T., Willshaw, D., 1992. Cerebellar cortex: its simulation and the relevance of Marr's theory. Philos. Trans. R. Soc. Lond. Ser. B Biol. Sci. 336, 239–257.

Vanier, M.T., 1983. Biochemical studies in Niemann-Pick disease. I. Major sphingolipids of liver and spleen. Biochim. Biophys. Acta 750, 178–184.

Vanier, M.T., 1999. Lipid changes in Niemann-Pick disease type C brain: personal experience and review of the literature. Neurochem. Res. 24, 481–489.

Vanier, M.T., 2010. Niemann-Pick disease type C. Orphanet J. Rare Dis. 5, 16.

Voikar, V., Rauvala, H., Ikonen, E., 2002. Cognitive deficit and development of motor impairment in a mouse model of Niemann-Pick type C disease. Behav. Brain Res. 132, 1–10.

vom Dahl, S., Mengel, E., 2010. Lysosomal storage diseases as differential diagnosis of hepatosplenomegaly. Best Pract. Res. Clin. Gastroenterol. 24, 619–628.

Wassif, C.A., Cross, J.L., Iben, J., Sanchez-Pulido, L., Cougnoux, A., Platt, F.M., Ory, D.S., Ponting, C.P., Bailey-Wilson, J.E., Biesecker, L.G., Porter, F.D., 2016. High incidence of unrecognized visceral/neurological late-onset Niemann-Pick disease, type C1, predicted by analysis of massively parallel sequencing data sets. Genet. Med. 18, 41–48.

Williams, A.L., Hoofnagle, J.H., 1988. Ratio of serum aspartate to alanine aminotransferase in chronic hepatitis. Relationship to cirrhosis. Gastroenterology 95, 734–739.

Wraith, J.E., Guffon, N., Rohrbach, M., Hwu, W.L., Korenke, G.C., Bembi, B., Luzy, C., Giorgino, R., Sedel, F., 2009. Natural history of Niemann-Pick disease type C in a multicentre observational retrospective cohort study. Mol. Genet. Metabol. 98, 250–254.

Wraith, J.E., Vecchio, D., Jacklin, E., Abel, L., Chadha-Boreham, H., Luzy, C., Giorgino, R., Patterson, M.C., 2010. Miglustat in adult and juvenile patients with Niemann-Pick disease type C: long-term data from a clinical trial. Mol. Genet. Metabol. 99, 351–357.

Xie, C., Turley, S.D., Dietschy, J.M., 1999. Cholesterol accumulation in tissues of the Niemann-pick type C mouse is determined by the rate of lipoprotein-cholesterol uptake through the coated-pit pathway in each organ. Proc. Natl. Acad. Sci. U.S.A. 96, 11992–11997.

https://doi.org/10.1016/j.heliyon.2019.e01293

Yanez, M.J., Belbin, O., Estrada, L.D., Leal, N., Contreras, P.S., Lleo, A., Burgos, P.V., Zanlungo, S., Alvarez, A.R., 2016. c-Abl links APP-BACE1 interaction promoting APP amyloidogenic processing in Niemann-Pick type C disease. Biochim. Biophys. Acta 1862, 2158−2167.

Zervas, M., Dobrenis, K., Walkley, S.U., 2001. Neurons in Niemann-Pick disease type C accumulate gangliosides as well as unesterified cholesterol and undergo dendritic and axonal alterations. J. Neuropathol. Exp. Neurol. 60, 49−64.

Zhang, M., Sun, M., Dwyer, N.K., Comly, M.E., Patel, S.C., Sundaram, R., Hanover, J.A., Blanchette-Mackie, E.J., 2003. Differential trafficking of the Niemann-Pick C1 and 2 proteins highlights distinct roles in late endocytic lipid trafficking. Acta Paediatr. 92, 63−73 discussion 45.

https://doi.org/10.1016/j.heliyon.2019.e01293